Energy Conversion and Management 199 (2019) 111956

Contents lists available at ScienceDirect

Energy Conversion and Management

journal homepage: www.elsevier.com/locate/enconman

Geothermal energy from flooded mines: Modeling of transient energy recovery with thermohaline stratification

Ting Bao[a,c,*], Zhen (Leo) Liu[b,*]

[a] Department of Civil and Environmental Engineering, Michigan Technological University, 1400 Townsend Drive, Dow 854, Houghton, MI 49931, United States
[b] Department of Civil and Environmental Engineering, Michigan Technological University, 1400 Townsend Drive, Dillman 201F, Houghton, MI 49931, United States
[c] Key Laboratory of Metallogenic Prediction of Nonferrous Metals and Geological Environment Monitoring (Central South University), Ministry of Education, 932 Lushan S Road, Changsha, Hunan 410083, China

ARTICLE INFO

Keywords:
Mine water
Thermohaline stratification stability
Heat extraction
Pumping rate
Open-loop system

ABSTRACT

Geothermal energy from flooded mines is a high-potential clean energy resource that can provide heating to large communities with power comparable to small-scale power plants. The transient energy recovery process for utilizing this energy resource, however, has not been well understood, especially those involving the heat transfer in mine water with the widely-observed layering phenomenon where the temperature and salinity are stratified. To better understand the transient energy recovery process considering such a layering phenomenon, this study presents a numerical analysis of transient heat extraction from a flooded mine shaft with mine water dominated by thermohaline stratification. The numerical analysis is conducted based on a realistic case using an open-loop heat pump system. The simulation results show that, when normal pumping rates are used, the water temperature available to heat pumps almost keeps unchanged because the transient energy recovery using an open-loop system only leads to a temperature reduction of 0.2–0.3 K. By comparison, the simulation results in this study are consistent with those measured from real demonstration projects, showing the accuracy of the simulations and confirming the high efficiency and reliability of this energy innovation. The modeling results in this study also reveal that heat extraction does not affect the stability of thermohaline stratification when normal pumping rates, e.g.,0.0014–0.03 m^3/s, are adopted, but will break thermohaline stratification with pumping rates over a hundred times of the commonly-used ones. These findings provide guidelines for future applications at different scales, and the methodology reported in this study can be used to assist the design of the energy recovery systems.

1. Introduction

Increasing consumption of energy for heating buildings, either domestically or commercially, has drawn worldwide attention to renewable energy resources. Compared to conventional energy resources, e.g., fossil fuels, renewable energy, e.g., solar energy [1], wind energy [2], bio-materials energy [3], hydropower energy [4], and geothermal energy [5], is more attractive because such types of energy are green, clean, sustainable, and eco-friendly. Among them, geothermal energy is gaining momentum worldwide because of its economic benefits [6] and its huge quantity of heat continuously generated by the Earth's interior [7]. To utilize geothermal energy, heat pumps with the ability to transfer heat from or to the ground are the most energy-efficient means of heating and cooling buildings in the world [8]. Three major types of heat pump systems are conventionally used for geothermal applications [9]: Ground-Water Heat Pump (GWHP), Ground-Coupled Heat Pump (GCHP), and Surface-Water Heat Pump (SWHP). SWHPs achieve heat exchange via heat convection of bulk water in a lake or a pond; therefore, heat transfer in SWHPs is more significant than that in GWHPs via heat convection of borehole water (not bulk water) and that in GCHPs via heat conduction between the ground and water pipes.

The use of water in flooded mines for geothermal applications is a variation of SWHPs and has been pioneered worldwide in recent years. Numerous underground mines around the world were flooded with water after their closure [10]. Because the great depths of mines provide high water temperatures contrast with the air temperature, abandoned flooded mines are potentially large-scale geothermal energy reservoirs for providing sustainable and low-enthalpy energy with low

* Corresponding authors at: Department of Civil and Environmental Engineering, Michigan Technological University, 1400 Townsend Drive, Dow 854, Houghton, MI 49931, United States (T. Bao). Department of Civil and Environmental Engineering, Michigan Technological University, 1400 Townsend Drive, Dillman 201F, Houghton, MI 49931, United States. Phone: (906) 487 1826; fax: (906) 487 1620 (Z. Liu).
E-mail addresses: tbao@mtu.edu (T. Bao), zhenl@mtu.edu (Z.L. Liu).

https://doi.org/10.1016/j.enconman.2019.111956
Received 17 June 2019; Received in revised form 14 August 2019; Accepted 16 August 2019
Available online 23 August 2019
0196-8904/

Nomenclature

$\boldsymbol{g}$	gravitational acceleration vector [m/s^2]
t	time [s]
p	total pressure [Pa]
p_d	hydrodynamic pressure [Pa]
T_0	reference temperature [K]
T	temperature [K]
T_{ref}^p	pumping reference temperature [K]
ΔT	temperature difference [K]
T_{in}	inlet temperature [K]
T_{out}	outlet temperature [K]
S_0	reference salinity [%, w/w]
S	salinity [%, w/w]
E_c	total energy [J]
E_t	total pumping energy [J]
$\boldsymbol{U}$	velocity [m/s]
A	cross-sectional area [m^2]
A_p	cross-sectional area of pipes [m^2]
$\dot{m}$	pumping rate [m^3/s]
V_A	cell volume [m^3]
Q_T^{in}	inlet energy rate [W]
Q_T^{out}	outlet energy rate [W]
Q_T	net energy rate [W]
c_p	specific heat [J/(kg K)]
u_p	pumping velocity [m/s]
z	elevation [m]

Dimensionless numbers

N	buoyancy ratio
M	cell number
i	cell index

Greek symbols

ρ	density [kg/m^3]
ρ_0	reference density [kg/m^3]
ν_{eff}	effective kinematic viscosity [m^2/s]
β_T	thermal expansion coefficient [K^{-1}]
β_S	solutal expansion coefficient [%$^{-1}$]
α_T	thermal eddy diffusivity [m^2/s]
α_{eff}^T	effective thermal diffusivity [m^2/s]
α_{eff}^S	effective solutal diffusivity [m^2/s]

carbon emissions [11] by means of heat pumps [12]. Since the pioneering geothermal recovery with mine water in Canada [13], this energy innovation has been pioneered in many real projects around the world, such as Germany [14], Scotland [15], the United Kingdom [16], and Netherlands [17]. In the U.S., a real project detailed in [18] has been running well for heating a 1394 m^2 building with mine water in a flooded copper mine using an open-loop heat pump system since 2009. Two other demonstration projects in Markham [19] and Overton [20] in the U.K. have also shown high levels of performance coefficients with an open-loop heat pump system for heating buildings. For real installations, the investment and economic payback are usually the major driving force. The designed annual thermal energy, in general, determines the investment. Installing a geothermal heating plant with 0.41 GWh/year thermal energy can cost about 0.33 million dollars [21]. According to Petričko et al. [22], the investment of installing a geothermal heating plant with 10 MW of power could be several million dollars with a payback period of about 17 years. 10 MW of power, in fact, can provide heating to multiple buildings for about 1,700 households [23]. The investment of installing a single-building geothermal system for heating, however, is around $100,000 and the payback can be achieved quickly within 3–5 years [18].

Besides the above-introduced real projects, many numerical and field studies have evaluated the heat reserves in mine water for geothermal applications. MaJolepszy [24] estimated that a maximum thermal power of 20 MW can be extracted over 50 years with a temperature reduction of 7–8 °C by modeling heat extraction from a flooded coal mine. Bailey et al. [25] predicted a thermal power of 47.5 MW available in mine water for geothermal applications in the coalfields of Great Britain. Jardón et al. [26] reported that 260,000 MWh can be annually extracted with mine water in a mine in central Asturias, Spain. In other mines in Spain, Menéndez et al. [23] estimated 20 MW of thermal power available for heat recovery. In addition, 38.1–120.8 MW could be recovered from the flooded Sierra Almagrera mines [27]. The above results revealed the great thermal potential for geothermal applications with mine water. In real applications, the temperature variation in mine water is a key to determining the efficiency and sustainability of the application. Loredo et al. [28] found that the mine water temperature almost remained unchanged during heat extraction based on the field data. Andrés et al. [29] also found that the mine water temperature was very stable during heat extraction via numerical simulations in a period of 90 years under different scenarios of water extraction and injection. These results showed that mine water is a very reliable resource for heat recovery. In addition to the heat potential assessments, numerical studies also have been conducted to understand the optimal and efficient use of mine water for heating. Raymond and Therrien [30] modeled the groundwater flow in flooded mines in Canada to investigate the long-term performance of geothermal energy recovery. They found that a sustainable water pumping rate for energy extraction was 0.049 m^3/s if the mine water temperature after heat extraction was 3 °C. Raymond and Therrien [31] investigated the optimal design of a heat pump system for the energy application and found that the minimum and maximum water pumping rates were 0.019 m^3/s and 0.063 m^3/s, respectively, by modeling groundwater flows and heat transfer in the mine-water-surrounding-formation system. However, all of the above-mentioned modeling studies treated mine water as a 1D flow; as a result, the realistic heat and mass transport in large bodies of mine water has not been well considered.

To date, a few numerical studies considered more realistic heat and mass transport mechanisms in mine water for modeling heat extraction. Madiseh et al. [32] investigated forced convection in mine water inside a tunnel at the bottom of a flooded mine for heat extraction. Thornton [33] analyzed the effect of the thermal convection in mine water to evaluate the heat exchanger placement and configuration in a vertical flooded mine shaft. Strictly speaking, these studies did not reveal the realistic heat and mass transport mechanisms in mine water due to the exclusion of salinity transport in mine water. Field measurements showed that the salinity in mine water is in a range of 65.4–610.4 ppm [34] and it will increase as the depth goes deeper because of the geochemical gradient [34,35]. Thus, the realistic mine water movement in most flooded mines is driven by a special heat and mass transport mechanism: Double-Diffusive Convection (DDC) [35]. The buoyancy force that drives mine water to move is affected by heat and salt transport with different diffusivities, where the distributions of heat and salinity affect the vertical density gradient of mine water in the opposite way [36]. Due to DDC, mine water has a distinctive feature that has been observed as a widely-existing phenomenon in mine water around the world, e.g., Germany [35], the U.K. [37], France [38], and the U.S. [39]. This feature is that temperature and salinity in mine water are stratified to form different layers along a mine shaft, which is termed thermohaline stratification. Each layer has almost the same

temperature and salinity. Significant heat and salinity gradients occur at the interface between two adjacent layers. To understand such thermohaline stratification, Reichart et al. [38] modeled the mine water movement dominated by DDC. However, thermohaline stratification was not successfully observed in the study [38]. Recently, Bao and Liu [40] succeeded in reproducing thermohaline stratification in large bodies of mine water via multiphysics simulations. The study [40] scientifically explained the formation of thermohaline stratification, where the structure of thermohaline stratification is consistent with those observed from field measurements. Despite the progress, no research has been reported on modeling heat extraction from real flooded mines considering thermohaline stratification.

Thermohaline stratification governed by DDC is, in fact, critical to the efficiency and sustainability of this energy application and thus cannot be overlooked. For heat extraction using an open-loop heat pump system (commonly used in mine water-based geothermal applications, e.g., [18,20]), one key consideration in the determination of the efficiency of heat pumps for extracting heat is the water temperature available to the heat pumps, which is determined by the water temperature distribution and pumping location. In addition, the variation of the temperature distribution (i.e., the structure of thermohaline stratification), which is affected by the pumping rate, pumping location, and natural heat and mass transport, will further determine the future water temperatures available to the heat pumps. This will determine both the efficiency and sustainability of the whole geothermal application. Therefore, thermohaline stratification interacts with the selection of geothermal energy system parameters (i.e., pumping rates and locations) in a very complicated way. One example is that heat extraction with a high pumping rate may affect the instability of thermohaline stratification by breaking thermohaline stratification. As a result, the water movement will mix heat and salts to alter water temperatures in a complex way. This may result in a significant reduction in water temperatures during heat extraction and consequently affect the sustainability of the whole energy application. However, the influence of such events on the stability of thermohaline stratification is still little known. Therefore, a sound understanding of the interaction between heat extraction and the natural heat and mass transport dominated by thermohaline stratification is not only highly desirable but also urgently needed.

To fill the above knowledge gaps, this study reports on a methodology to simulate transient heat extraction from a single mine shaft via an open-loop system based on unique non-isothermal and non-isosolutal hydrodynamics. The objectives are to (1) simulate transient heat extraction considering thermohaline stratification and (2) reveal the influence of heat extraction on the stability of thermohaline stratification. The study is organized as follows. A scientific framework with unique non-isothermal and non-isosolutal hydrodynamics for modeling heat extraction is presented first and then validated against theoretical results. After that, heat extraction simulation is conducted based on a realistic mine shaft using the validated model. Based on the simulation, the performance of heat extraction considering thermohaline stratification is evaluated, and the influence of heat extraction on the stability of thermohaline stratification is discussed.

2. Theory and method

2.1. Mathematical formulation

2.1.1. Mine water governing equation

The governing equations for DDC in mine water, including the continuity equation, momentum equation, energy equation, and salinity equation, are formulated as

$$\begin{cases} \frac{\partial \rho_0}{\partial t} + \nabla\cdot(\rho_0 \boldsymbol{U}) = 0 \\ \frac{\partial \boldsymbol{U}}{\partial t} + \boldsymbol{U}\cdot\nabla\boldsymbol{U} = -\frac{\nabla p_d}{\rho_0} + \nabla\cdot(\nu_{eff}\nabla\boldsymbol{U}) - \frac{\rho}{\rho_0}\boldsymbol{g} \\ \frac{\partial T}{\partial t} + \boldsymbol{U}\cdot\nabla T = \nabla\cdot(\alpha_{eff}^{T}\nabla T) \\ \frac{\partial S}{\partial t} + \boldsymbol{U}\cdot\nabla S = \nabla\cdot(\alpha_{eff}^{S}\nabla S) \end{cases} \quad (1)$$

where $\boldsymbol{U}$ is the mine water velocity; t is the time; ρ_0 is the reference mine water density; ν_{eff} is the effective viscosity; ρ is the mine water density; p_d is the dynamic pressure, in which $p_d = p - \rho g z$; z is the elevation; p is the total pressure; $\boldsymbol{g}$ is the acceleration vector; the absolute value of $\rho g z$ is the static pressure; T is the mine water temperature; α_{eff}^{T} is the effective thermal diffusivity; S is the salinity; and α_{eff}^{S} is the effective solutal diffusivity. To consider the buoyancy force induced by temperature and salinity differences, the Oberbeck-Boussinesq approximation [41] was used, where the density ρ is assumed to vary linearly with the temperature T and salinity S

$$\rho = \rho_0[1 - \beta_T(T - T_0) + \beta_S(S - S_0)] \quad (2)$$

where β_T is the coefficient of thermal expansion; β_S is the coefficient of solutal expansion; and T_0 and S_0 are the reference temperature and salinity, respectively. To consider the influence of salinity and temperature on the buoyancy force, the buoyancy ratio N defined by Eq. (3) was adopted

$$N = \frac{\beta_S \Delta S}{\beta_T \Delta T} \quad (3)$$

where ΔT and ΔS are the temperature difference and salinity difference, respectively.

Turbulent flow is common in mine water [35]. Bao and Liu [40] also confirmed that the turbulence was needed to successfully reproduce thermohaline stratification. For modeling large-scale water movements in oceans, constant transport parameters are widely adopted [42]. Based on this fact, this study assumed constant values of the effective kinematic viscosity and effective diffusivity for large water mine bodies. For both thermal and solutal diffusion, the effective diffusivity is the sum of the eddy diffusivity and the laminar diffusivity. Thermal eddy diffusivity α_T can be estimated using the below equation [43]

$$\boldsymbol{U}'T' = -\alpha_T \nabla T \quad (4)$$

where $\boldsymbol{U}'T'$ is the eddy flux. According to Wolkersdorfer [35], the maximum velocity of mine water measured from tracer tests was in the order of 10^{-2} m/s. α_T thus can be estimated with this velocity magnitude. Other parameters, including the solutal eddy diffusivity, effective kinematic viscosity, and eddy kinematic viscosity, are also needed. To obtain such parameters, this study adopted the same calculations used and detailed in [40]. The values of all of the transport parameters will be presented in Section 3.1.

2.1.2. Heat extraction formulation

For heat extraction, an open-loop heat pump system is commonly used in real geothermal applications with mine water (e.g., [20]). At a pumping location, the pumping velocity u_p can be calculated as

$$u_p = \frac{\dot{m}}{A_p} \quad (5)$$

where $\dot{m}$ is the volumetric flow rate, and A_p is the cross-sectional area of a pumping pipe. The power extracted from mine water by an open-loop heat pump system can be calculated using the following equation

$$\begin{cases} Q_T^{out} = \dot{m}\rho c_p(T_{out} - T_{ref}^{p}) & \text{leaving (outlet)} \\ Q_T^{in} = \dot{m}\rho c_p(T_{ref}^{p} - T_{in}) & \text{returning (inlet)} \end{cases} \quad (6)$$

where c_p is the water specific heat; T_{out} is the outlet mine water temperature (i.e., pumped water temperature); Q_T^{out} is the power at the outlet; T_{in} is the inlet mine water temperature (i.e., water temperature

after heat extraction); Q_T^{in} is the power at the inlet; and T_{ref}^{p} is the reference pumping temperature. This reference pumping temperature is used to eliminate the numerical stability issue as a great temperature gradient will occur at the outlet if $Q_T^{out} = \dot{m}\rho c_p T_{out}$ is used directly. To avoid this stability issue, T_{ref}^{p} is defined as T_{out}. Therefore, Q_T^{out} is equal to zero at the outlet. At the inlet, the energy rate from mine water is formulated as

$$Q_T = \dot{m}\rho c_p (T_{out} - T_{in}) \tag{7}$$

where Q_T is the net energy rate at the inlet.

2.2. Numerical framework implementation

The governing equations presented in Section 2.1.1 were implemented with the finite volume method using a C++ open source platform, OpenFOAM. A new solver, *DDCFoam,* was developed by coding for solving the governing equations to simulate a double-diffusive flow triggered by temperature and salinity differences. For the spatial discretization, the Gauss linear scheme with the second-order accuracy [44] was utilized to discretize the Laplacian and gradient terms based on Gauss' theorem. Take the Laplacian term in Eq. (1), i.e., $\nabla\cdot(\alpha_{eff}^{T}\nabla T)$, as an example, its discretization form is expressed as

$$\int_{V_P} \nabla\cdot(\alpha_{eff}^{T}\nabla T)dV = \int_{F} d\boldsymbol{F}\cdot(\alpha_{eff}^{T}\nabla T) = \sum_{f=1}^{\xi} (\alpha_{eff}^{T})_f |F_f| \frac{T_I - T_J}{|\boldsymbol{d}_f|} \tag{8}$$

where V_P is the control volume, F_f is the face area, ξ is the number of faces of V_P, I and J are the centroids for two adjacent volume cells, and $\boldsymbol{d}_f$ is the distance vector. For the temporal discretization, the Euler scheme with the first-order accuracy [44] was used to discretize the accumulation term, e.g., $\frac{\partial S}{\partial t}$ as

$$\frac{\partial}{\partial t}\int_{V_P} SdV = \int_{V_P} \frac{S_I - S_I^o}{\Delta t}dV = \frac{S_I - S_I^o}{\Delta t}V_P \tag{9}$$

where the superscript "o" represents the old-time step value. The PIMPLE algorithm [45] was adopted for numerical iterations. For the convergence criterion, the iterative calculation is stopped when all the final residuals for velocity, salinity, and enthalpy fall below a preset tolerance of 10^{-7}.

2.3. Numerical framework validation

The framework developed in Section 2.1 is validated in this section. The framework validation is fulfilled in two separate parts. The first part is to validate the accuracy of DDC without heat extraction, which is compared to the documented results [46]. Details of the first part will not be repeated here but can be found in [40]. The second part is to validate transient heat extraction from the dynamic DDC system, which can be accomplished against the theoretical results. Details of the second part are presented in the following.

Fig. 1 shows the schematic of the 2D model configuration for validating transient heat extraction from the dynamic DDC system. The model was configured with a water depth of 50 m. The size of finite volume cells was 0.36 m in the horizontal direction and 0.4 m in the vertical direction. To consider heat extraction via an open-loop system, two finite volume cells (rectangular elements in this 2D model) in the water domain were removed, leading to two "blank" rectangular areas, as shown in Fig. 1. These two areas are filled with no water and are thus cavities. Their faces were treated as external boundaries. This model set-up is similar to that of heat extraction from a geothermal standing column well using an open-loop system used in Abu-Nada et al. [47] and Al-Sarkhi et al. [48]. The inlet was prescribed at the bottom boundary of the upper cavity (i.e., the green one) to consider the returning mine water after heat extraction. The outlet was set up at the bottom boundary of the lower cavity (i.e., the red one) to consider the leaving mine water to a heat exchanger. Mathematically, the initial and boundary conditions to consider the above heat extraction process can be described using the following equations

$$\begin{cases} T = 300\,K,\ S = 0.01\% & \text{at t=0} \\ T_{in} = 295\,K\ ,\ \nabla S = 0 & \text{at the inlet} \\ \nabla T = 0,\ \nabla S = 0 & \text{at the outlet} \\ U_x = 0,\ U_z = -0.005\,\text{m/s} & \text{at the inlet} \\ U_x = 0,\ U_z = 0.005\,\text{m/s} & \text{at the outlet} \end{cases} \tag{10}$$

It is noted that there are no thermal and solutal fluxes on other boundaries of these two cavities (i.e., boundaries except the outlet and inlet) and all boundaries of the water domain (see Fig. 1). T_{in} = 295 K and $\nabla T = 0$ were defined at the inlet and outlet, respectively, to ensure that a temperature loss of 5 K occurs due to heat extraction with the heat exchanger. Accordingly, the total extracted energy amount E_c during any computing periods can be computed by

$$E_c = \sum_{i}^{M} \rho c_p V_A \Delta T_i \tag{11}$$

where i is the cell index; M is the total number of cells; V_A is the volume (i.e., 0.144 m^3) of the cell with a unit thickness; and ΔT_i is the temperature difference of the cell i within a certain computing period t.

Theoretically, the total energy E_t extracted from the mine water environment within the same computing period can be calculated by

$$E_t = \dot{m}\rho c_p t\Delta T \tag{12}$$

where ΔT is the temperature difference (i.e., 5 K). $\dot{m}$ for this 2-D case can be calculated by multiplying U_z by the horizontal length of the cell (i.e., 0.36 m) and a unit thickness in the z-direction. For the validation, the theoretical results computed with Eq. (12) are compared with the numerical results computed with Eq. (11). As shown in Fig. 2, the ratios between the theoretical and numerical results are almost equal to 1.0 at different times. This good agreement demonstrates the good capacity and accuracy of the developed framework for calculating the output energy via transient heat extraction from the DDC system using an open-loop system.

2.4. Site description and corresponding heat extraction model set-up

Transient heat extraction from a real copper mine shaft considering thermohaline stratification was simulated using the numerical framework validated in Section 2.3. The Upper Peninsula of Michigan shown

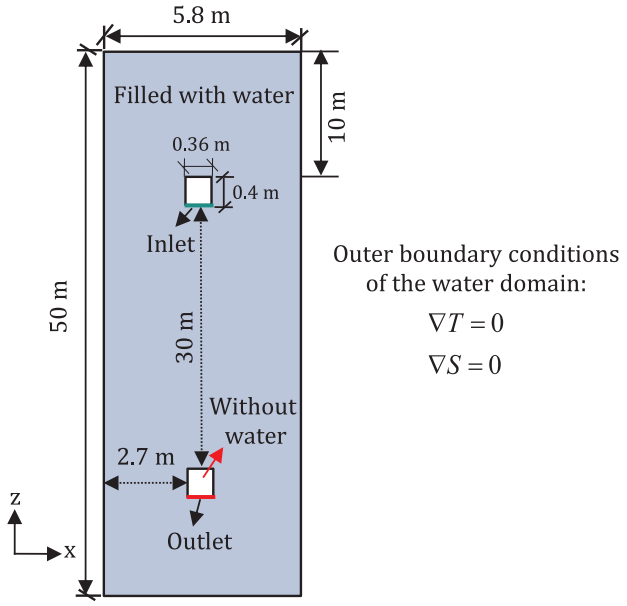

Fig. 1. Configuration of the model for validating transient heat extraction.

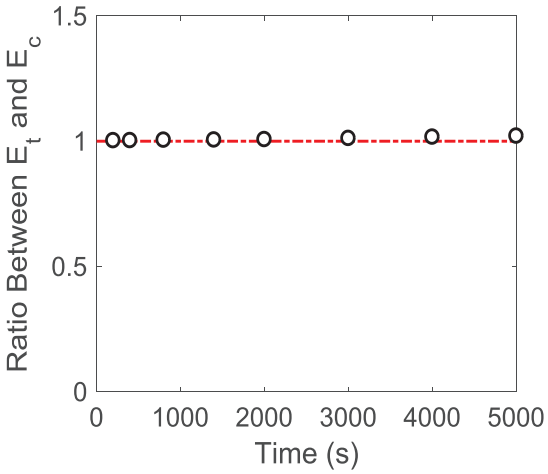

Fig. 2. Comparison between the theoretical results and the numerical results.

in Fig. 3 was a historical copper mining area with over 3150 past underground mines according to the United States Geological Survey [49]. Among them, the Hancock mine is located in the city of Hancock, where the community thrived within 1 km of the mine (see Fig. 3). Therefore, the use of this mine for heating can compensate the expenditure for water pumping work and energy delivery. According to field observations in Hancock Shaft 2 [39], there are at least two stratified temperature layers in mine water in Shaft 2 with a temperature range of 9–15.2 °C, which is suitable for geothermal applications for heating [18]. Therefore, Hancock Shaft 2 was chosen for the following simulation.

Fig. 4 shows the configuration of a 2D model (Fig. 4b) developed based on the layout of the mine (Fig. 4a). The model includes one vertical shaft with a depth of 1159.2 m and eight horizontal drifts with a length of 50 m, in which the length of drifts was configured shorter than the actual ones to save computational cost. The geometric model was meshed via structured grids with a size of 0.36 m and 0.4 m in the horizontal and vertical directions, respectively (Fig. 4c). For regions on boundaries, a small grid size of 0.01 m was used to avoid stability issues when considering lateral heat fluxes from the surroundings, because a relatively large grid size, e.g., 0.4 m, will cause stability issues. 65,446 cells were generated in total. It is noted that thermohaline stratification could not be observed if a low grid resolution, e.g., 1 m, was used [40]. The flow pattern thus depends on the grid size and a small grid size is recommended. To consider heat extraction, as shown in Fig. 4b, the inlet and outlet were set up on the external boundaries of two cavities, which is the same as the model set-up in Fig. 1. Mine water is pumped out at the outlet (i.e., the bottom boundary of the lower cavity in Fig. 4b) to an external heat exchanger and sent back into the shaft at the inlet (i.e., the bottom boundary of the upper cavity) after heat

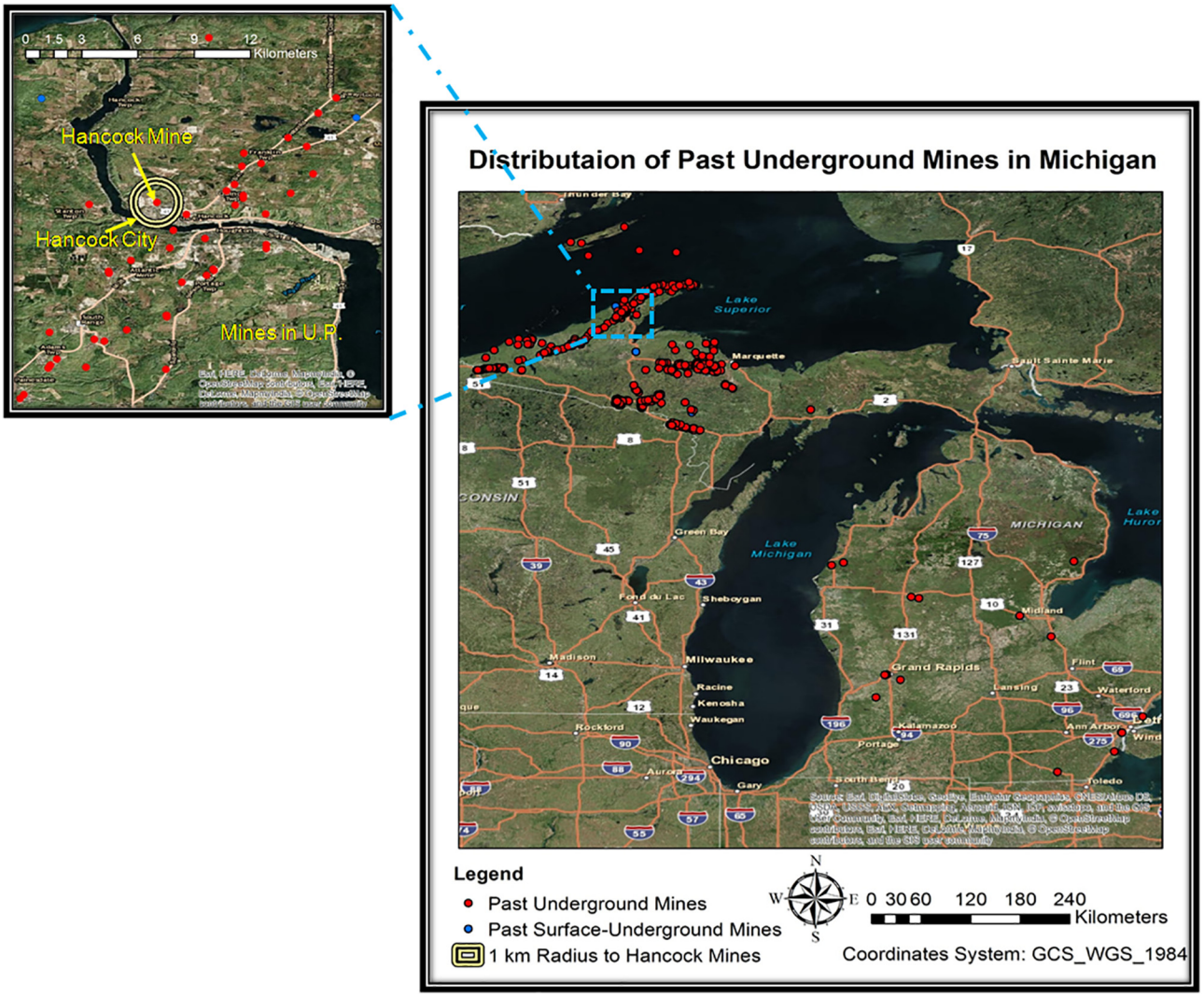

Fig. 3. Past underground mines in Michigan and the location of the Hancock mine. Data is from USGS.

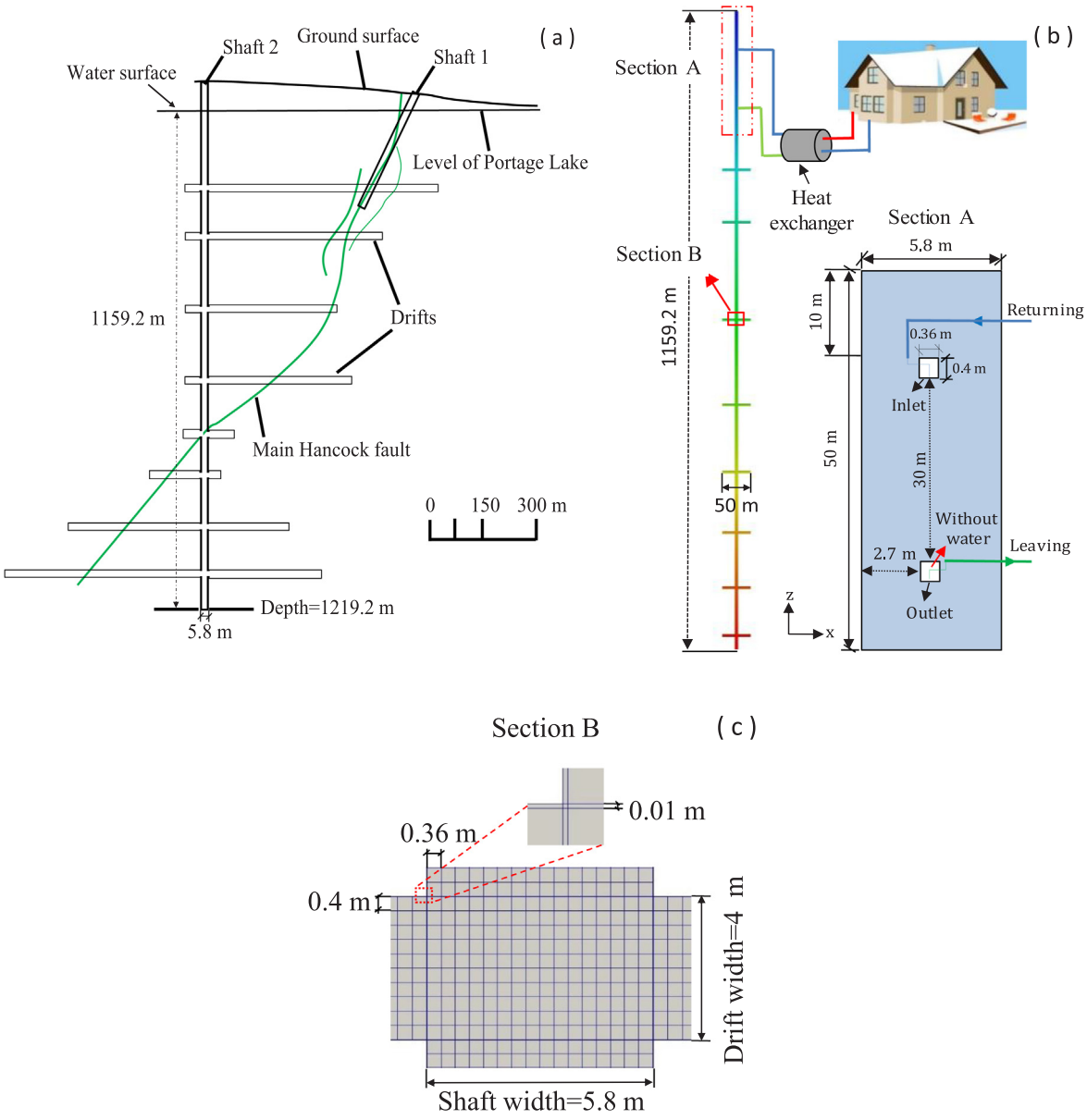

Fig. 4. Hancock Shaft 2: (a) underground structure layout [39], (b) simulation model configuration with heat extraction using an open-loop heat pump system and (c) geometry grids.

extraction using an open-loop system. The boundary conditions for the outlet and inlet are formulated as

$$\begin{cases} T = T_{in}, \nabla S = 0 & \text{at the inlet} \\ \nabla T = 0, \nabla S = 0 & \text{at the outlet} \\ U_x = 0, U_z = -\frac{\dot{m}}{A} & \text{at the inlet} \\ U_x = 0, U_z = \frac{\dot{m}}{A} & \text{at the outlet} \end{cases} \quad (13)$$

where A is the cross-sectional area (i.e., 0.36 m^2/s) and T_{in} is the inlet water temperature. The boundary conditions for mine water in Shaft 2 were the same as those used in [40], except that the present model only considered the heat flux as the lateral intrusion to the boundaries in the lateral directions. Two lateral heat fluxes were considered, one from the surrounding rocks and the other from the water flows through cracks and fissures in the surrounding rocks. A flux difference was also considered in the water flows through cracks and fissures between two lateral boundaries as this condition is required for successfully reproducing thermohaline stratification [40]. The lateral boundary condition for water velocity was set up to be non-slip because of the water-rock interface. More detailed explanations for the implementation of lateral boundary conditions can be found in [40].

For initial conditions, as shown in Fig. 5, three temperature and salinity layers were assumed to consider the thermohaline stratification that is present prior to heat extraction. Such initial conditions were obtained by running transient simulation without heat extraction, in which the initial temperature and salinity conditions were linearly distributed with the water depth according to field measurements [39] (i.e., 282.15 K to 288.35 K for temperature and 0.01% to 0.61% for salinity). A sodium chloride solution was adopted to represent the salinity in mine water as sodium chloride is the primary salt in mine water according to field measurements for chemical concentrations [39]. To consider representative pumping conditions for extracting heat, 0.0014 m^3/s (22.2 gpm), 0.0076 m^3/s (210.5 gpm), and 0.03 m^3/s (475.5 gpm) were chosen to consider low, medium, and high pumping rates, respectively, where the low and medium pumping rates were obtained according to a real application in [18] and the high pumping

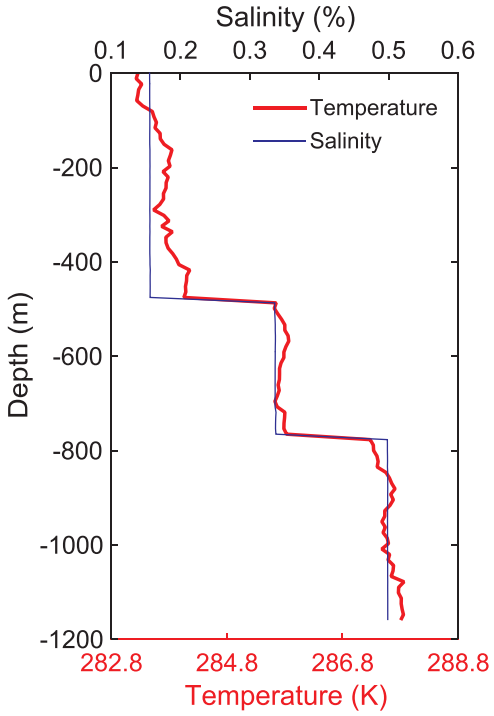

Fig. 5. Initial temperature and salinity distributions in mine water along the center axis of Shaft 2 for heat extraction.

rate was adopted according to a real application in [20]. Transient heat extraction lasting a week was simulated to compare the inlet and outlet water temperature variations in the simulation with those weekly measured from a real running project in the U.K. [20]. The parameters used in the simulation are tabulated in Table 1. A small time-step of 0.08 s was adopted to avoid stability issues when running the simulation.

3. Results

3.1. Heat extraction using an open-loop system

This section presents the transient simulation results of heat extraction from mine water considering thermohaline stratification. The temperature distributions of mine water at different times during heat extraction are shown in Fig. 6. Since the dimensions of mine water are too large to clearly visualize, the water depth range between 0 and 50 m containing the inlet and outlet areas was selected for visualization.

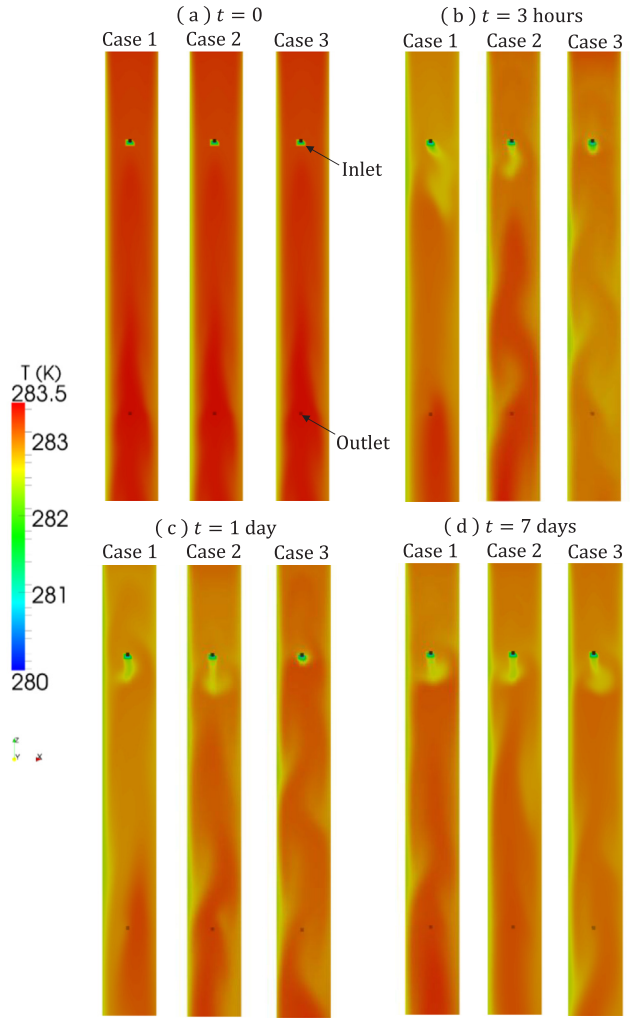

Fig. 6. Temperature color maps within the water depth range between 0 and 50 m with heat extraction at (a) 0, (b) 3 h, (c) 1 day, and (d) 7 days.

It is seen in Fig. 6a that the initial water temperature is almost 283.3 K everywhere except the inlet where 278.3 K was defined to consider heat extraction. Heat extraction leads to a clear water temperature reduction, as shown in Fig. 6b, c, and d. The temperature reduction is obvious in the region close to the inlet. At the outlet, the

Table 1
Parameters for mine water and the heat pump system used in the simulation.

Region	Parameter	Value		
Mine water	Reference density (kg/m^3)	1088.6		
	Reference temperature (K)	333.15		
	Reference salinity (%)	15		
	Specific heat (J/(kg K))	4181		
	Effective viscosity (m^2/s)	3.95×10^{-3}		
	Thermal expansion coefficient (K^{-1})	5.24×10^{-4}		
	Solutal expansion coefficient (%$^{-1}$)	6.82×10^{-3}		
	Effective thermal diffusivity (m^2/s)	4.94×10^{-4}		
	Effective salty diffusivity (m^2/s)	1×10^{-6}		
	Buoyancy ratio	1.26		
Open-loop heat exchanger		Case 1	Case 2	Case 3
	Volumetric flow rate (m^3/s)	0.0014	0.0076	0.03
	Inlet velocity (m/s)	−0.004	−0.021	−0.083
	Outlet velocity (m/s)	0.004	0.021	0.083
	Inlet temperature (K)	278.3		

Note: Thermal and solutal properties of mine water were determined according to Suárez et al. [50].

temperature slightly decreases, where the absolute value for the temperature decrease is less than 0.5 K during the simulated period for all the cases. This is because $Q_T^{out} = 0$ in Eq. (6) was defined, therefore, there is no heat loss when pumping water out at the outlet. As a result, the water temperature at the outlet only changes with the water movement caused by the returning water intruded from the inlet with the low temperature after heat extraction.

For velocity, the pumping velocity at the inlet induces the strong water movement to influence the water temperature distribution and variation in the whole mine water domain by driving the low water temperature from the inlet. To understand this, Fig. 7 shows the velocity profiles corresponding to the temperature color maps in Fig. 6. We can see in Fig. 7 that, for the three cases, the pumping velocity at the inlet causes the strong water movement in the region close to the inlet. This can be clearly seen in the zoom-in views of the inlet in Fig. 8. Due to the pumping action, the pumping velocity at the inlet (downward) changed the direction of the background water velocity in the natural mine water DDC movement from upward to downward. However, this pumping velocity, even for the value of 0.083 m/s calculated with the highest pumping rate (i.e., Cases 3) in Table 1, is lower than the background velocity. Therefore, the background velocity is only significantly altered in the region that is very close to the inlet, while the overall background water movement is negligibly affected. During the heat extraction, the low water temperature from the inlet (after heat extraction) is mixed quickly due to the background water movement, leading to a negligible temperature reduction in mine water (see Fig. 6). At the outlet, as shown in Fig. 8, no inversion for the water velocity direction is observed because the pumping velocity at the outlet and the background velocity have the same moving direction, i.e., upward.

For heat extraction, the outlet water temperature determines the efficiency and reliability of the heat pumps and is thus of practical interest. The outlet water temperature variations with time for the three cases are presented in Fig. 9a. The outlet water temperature almost remains unchanged at around 283.1 K, regardless of the pumping rates. For all the cases, the daily root-mean-square (RMS) average of the outlet temperature is in a range of 282.97–283.23 K (Fig. 9c). The above results indicate the high reliability of the energy application for heating. The inlet water temperature is also plotted in Fig. 9a, in which its value is a constant value because the water temperature at the inlet was fixed at 278. 3 K in the simulations. Based on the outlet water temperature in Fig. 9a, the temperature differences between the inlet and outlet for the three cases are plotted in Fig. 9b. All temperature reductions are located in the range of 4.6–5.1 K during the simulated period. This validates the high efficiency of the open-loop system to provide sufficient heating energy (4 K temperature reduction for a typical application [18]).

The above high efficiency and reliability of heat extraction can also be supported by the average water temperature within the water depth range between 0 and 50 m and water temperature comparisons with measurements from a real application. For the average temperature in mine water, as shown in Fig. 10, the average water temperature within the adopted water depth range is almost a constant, i.e., 283 K, which is about 0.3 K lower than the initial water temperature without heat extraction. The temperature reduction in this water depth range is only caused by the low temperature from the inlet. Though the inlet water temperature is 278. 3 K, as shown in Fig. 10, the water temperature at the location adjacent to the inlet (i.e., the finite volume cell next to inlet) is in the range of 280.2–282.2 K for the three cases. Fig. 11 presents the comparisons between the simulated outlet water temperatures for Case 1 and weekly measured inlet and outlet water temperatures in the Inman shaft building in the U.K. [20]. It is clearly seen that the variations of the simulated outlet water temperatures in this study confirmed the small temperature variations that have been measured in a real application during two monitoring weeks. That is, the outlet water temperature only changes slightly, i.e., 0.3–1 K, depending on the heating demand during the system operation [20]. Such temperature variations during geothermal energy recovery have been reported in demonstrations projects, e.g., [18,20], but have never been successfully obtained in numerical simulations before the current study.

The extracted heat from mine water and the remaining heat in the natural water system are also a practical interest in the energy application. Shown in Fig. 12 is the total extracted heat for the three cases, where the extracted heat is calculated with Eq. (10) based on the temperature difference obtained from Fig. 9b. Since the heat is extracted continuously, the extracted heat clearly increases with time. At the same operation time, the higher the pumping rate, the more the extracted energy. For remaining heat in the mine water environment after heat extraction, as shown in Fig. 12, the reaming heat computed with Eq. (11) for Case 3 (i.e., the highest pumping rate in Table 1) for the whole mine water body is almost the same as that without heat extraction after the simulated period, further validating the reliability of heat extraction with mine water for heating.

3.2. Stability of thermohaline stratification with heat extraction

As mentioned in the Introduction section, the variation of the temperature distribution (i.e., the structure of thermohaline stratification), especially those during heat extraction, determines the future water temperatures available to heat pumps and thus the sustainability of the whole energy application. To understand the evolution of thermohaline stratification affected by heat extraction, this section presents the results for the influence of heat extraction on the stability of

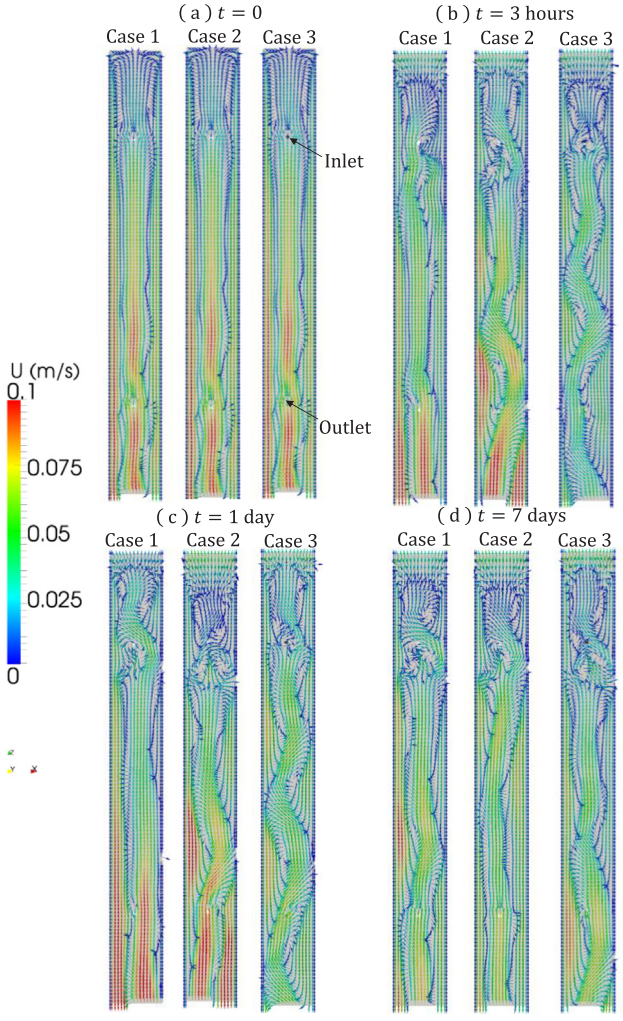

Fig. 7. Velocity profiles within the water depth range between 0 and 50 m during heat extraction at (a) 0, (b) 3 h, (c) 1 day, and (d) 7 days.

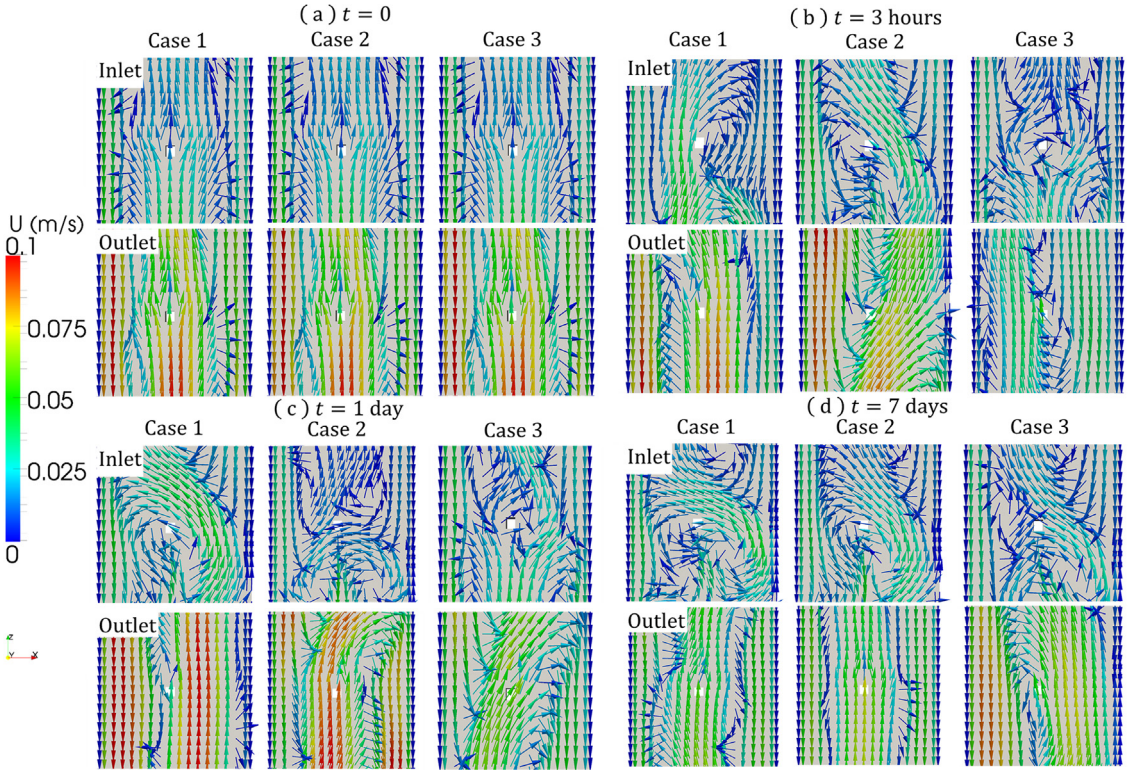

Fig. 8. Zoom-in views of velocity profiles at the inlet and outlet during heat extraction at (a) 0, (b) 3 h, (c) 1 day, and (d) 7 days.

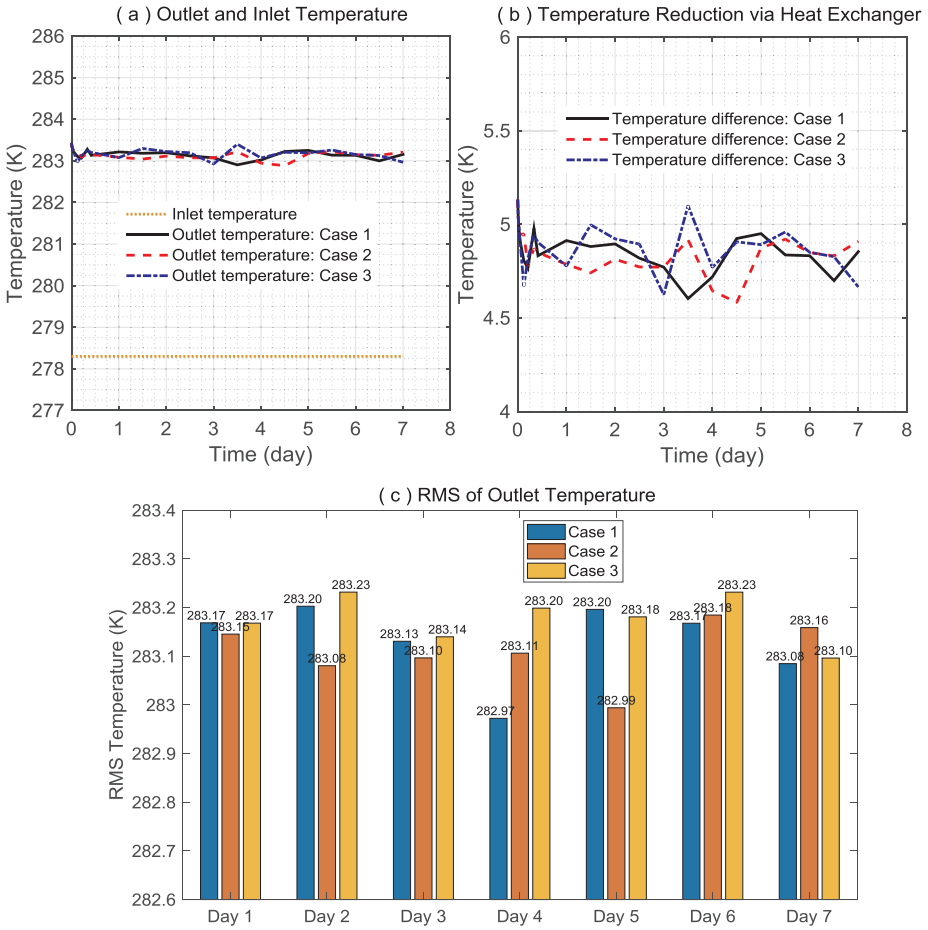

Fig. 9. Mine water temperatures at the inlet and outlet: (a) temperature variations, (b) temperature reductions through the heat exchanger, and (c) daily RMS of outlet temperatures presented in (a).

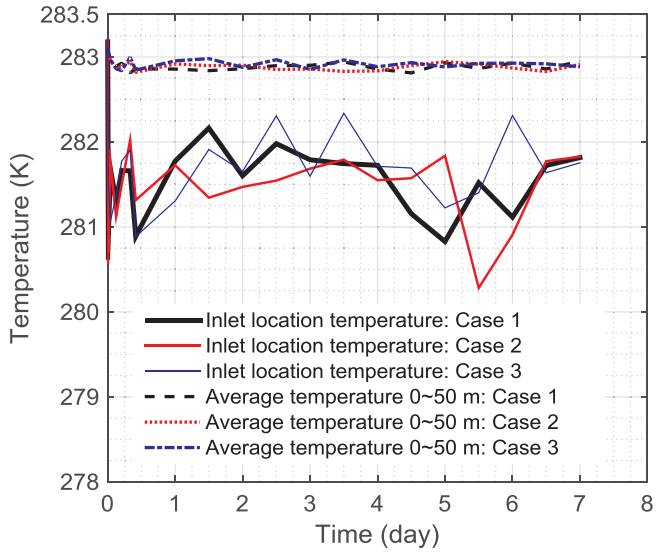

Fig. 10. Average mine water temperature within the water depth range of 0–50 m.

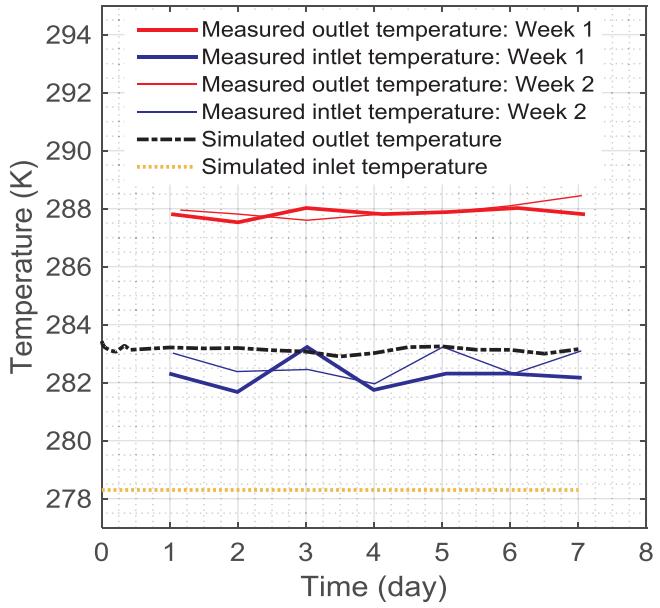

Fig. 11. Comparisons of the simulated outlet temperature for Case 1 with weekly measured outlet temperatures in the Inman shaft building in the U.K. [20].

thermohaline stratification with the three pumping rates in Table 1. The consequent structures of thermohaline stratification including that without heat extraction were compared to assess the influence of the pumping rate on the stability of thermohaline stratification.

For salinity, Fig. 13 plots the salinity distributions along the center axis of Hancock Shaft 2 with and without heat extraction at different times. It is clearly seen that the salinity distributions with heat extraction almost overlap that without heat extraction, regardless of the pumping rates for extracting heat. In the zoom-in views for the water depth range (i.e., 0–50 m) containing the pumping location, there is a difference in the salinity distributions. This difference is mainly caused by the pumping process at the inlet where the water with a low temperature is pumped back and impacts the natural DDC water movement after heat extraction. However, this difference is negligible, especially for Case 1, where the lowest pumping rate of 0.0014 m^3/s was adopted. The results in Fig. 13 imply that the heat extraction process has a

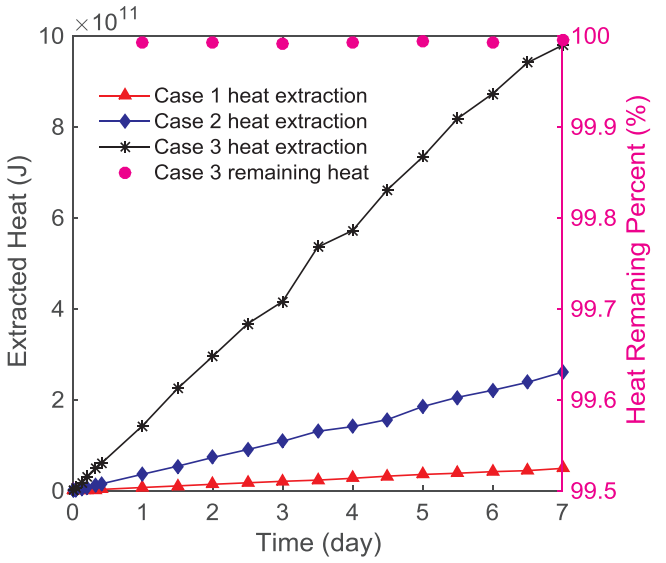

Fig. 12. Total extracted heat for the three cases from mine water in Hancock Shaft 2 using an open-loop system and the percent of heat remaining in the mine water environment after heat extraction.

negligible effect on the stability of salinity layers.

As for temperature, Fig. 14 presents the corresponding temperature distributions. The temperature distributions with heat extraction in the three cases are close to that without heat extraction. However, a significant difference in the temperature distributions in the top layer can be observed when heat extraction is in progress. As shown in the zoom-in views in Fig. 14, the water temperature with heat extraction at the pumping location (i.e., inlet) is about 0.25–0.4 K lower than that without heat extraction. Accordingly, the water temperatures during heat extraction are in the low-temperature range (left) while the water temperatures without heat extraction are in the relatively high-temperature range (right). However, this change for temperature distributions is only obvious in the top layer. The water temperature distributions with and without heat extraction in the middle and bottom layers are almost the same. Therefore, the stability of temperature layers is also hardly influenced by heat extraction. This can also be supported by the evolution of the absolute vertical temperature gradient along the center axis of Hancock Shaft 2. As shown in Fig. 15, the maximum water temperature gradient occurs at nearly the same water depth as time elapses, no matter heat extraction is in progress or not. This water depth is the location with the layer interface plotted in Fig. 14. It is clearly seen that the layer interface remains unchanged with time. According to the observations in Figs. 13–15, the influence of heat extraction on the stability of thermohaline stratification is negligible when the three pumping rates in Table 1 are adopted.

4. Discussions

The variations and distributions of the water temperature in Figs. 9–11 further prove the accuracy of the transient simulation of heat extraction in this study and confirm the reliability of the energy innovation with mine water. The outlet water temperature almost remains unchanged during heat extraction (see Fig. 9a), which is highly consistent with the measurements from real energy applications, e.g., [20,18]. The major reason is that the heat reserved in mine water is not "static", but can be replenished by heat fluxes from the surroundings (e.g., rocks and flows through rocks, see details in [40,51]). Therefore, the outlet water temperature will be heated not only by the flux from the lower portion of mine water but also those from the surroundings. Mine water performs like a "battery" with the energy replenishment for providing heating during heat extraction rather than a water reservoir

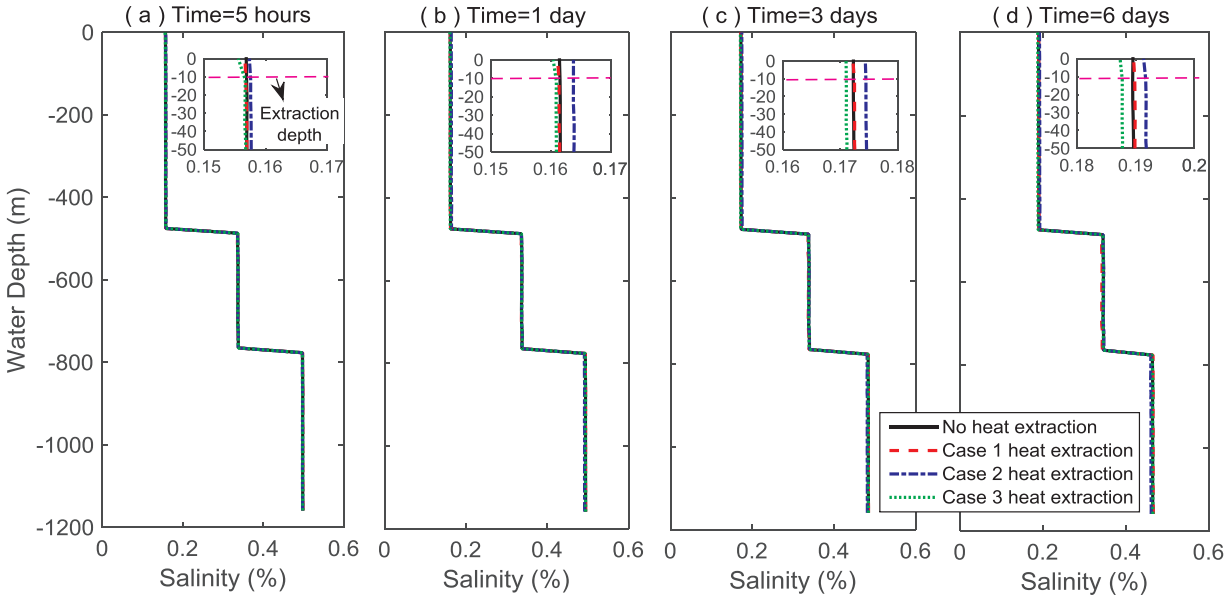

Fig. 13. Salinity distributions along the center axis of Hancock Shaft 2 with and without heat extraction at (a) 5 h, (b) 1 day, (c) 3 days, and (d) 6 days.

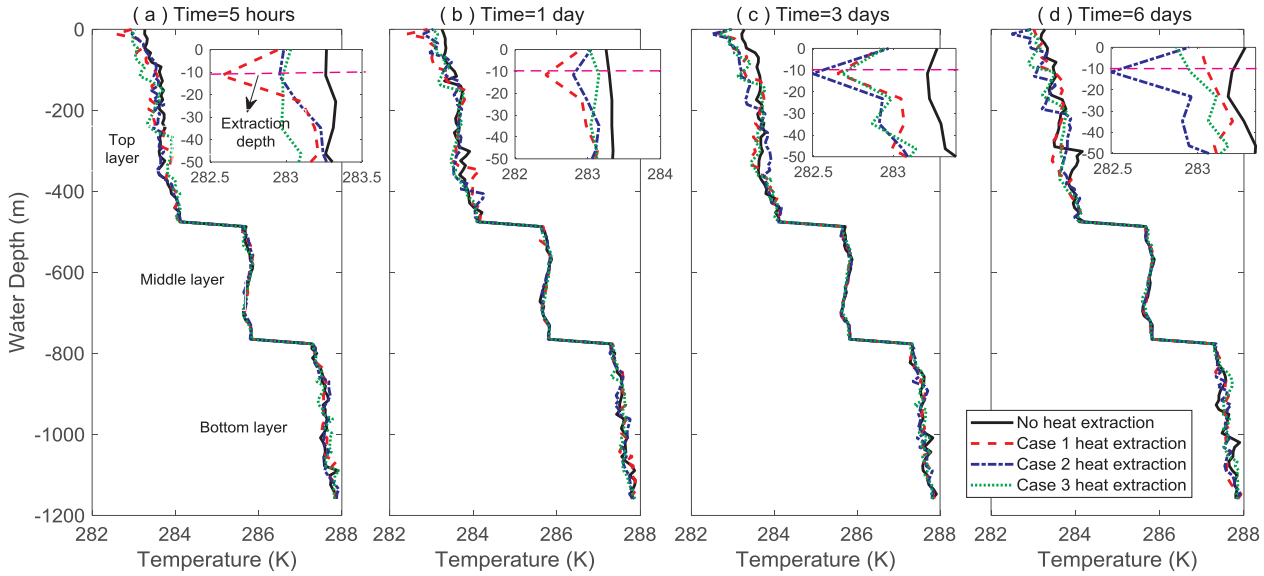

Fig. 14. Temperature distributions along the center axis of Hancock Shaft 2 with and without heat extraction at (a) 5 h, (b) 1 day, (c) 3 days, and (d) 6 days.

with only a static energy reserve.

The negligible influence of heat extraction on the stability of thermohaline stratification is mainly attributed to two facts. First, the pumping location (10 m) is very far from the water depth of the layer interface (about 480 m, see Fig. 15a). Due to this far distance, the low water temperature from the inlet after heat extraction can hardly affect the layer interface as the inlet water with the low water temperature has been well mixed by the surrounding water. Second, the pumping velocity is lower than the background water velocity, which can be clearly observed from the flow patterns in Figs. 7 and 8. The maximum background velocity in the DDC water movement is about 0.09 m/s, which is consistent with the typical maximum measured velocity of mine water from most of the tracer tests, e.g., Wolkersdorfer [35] and Kories et al. [52]. However, even for the highest pumping rate in Table 1, the corresponding pumping velocity is 0.083 m/s. Therefore, the background water movement primarily controls the temperature mixing in large bodies of mine water. This finding confirms that the existing geothermal applications with mine water, which use relatively small pumping rates (i.e., small scale), can run a long time without losing efficiency due to the drop in the temperature of mine water.

Increasing the pumping velocity to a very high pumping rate (e.g., 0.063 m^3/s according to [31]) may break the layer interface by significantly changing the flow patterns governed by natural DDC. To examine this possibility, three high pumping rates of 0.063 m^3/s, 0.142 m^3/s, and 0.284 m^3/s were further considered. As shown in Fig. 16, heat extraction breaks the interface between the top and middle layers when 0.142 m^3/s and 0.284 m^3/s are adopted. However, the layer interface still exists when 0.063 m^3/s is considered. The water temperature distributions under 0.142 m^3/s and 0.284 m^3/s are almost linear with the depth of 800 m.

For temperature variations, as shown in Fig. 17a, the outlet water temperature is in a range of 280–283 K, in which the temperature is higher if a lower pumping rate is adopted. In Fig. 17b, the water temperature differences between the outlet and inlet for these three high pumping rates are about 4.5 K, 3.6 K, and 3.2 K, which are lower than those with a relatively low pumping rate in Fig. 9b.

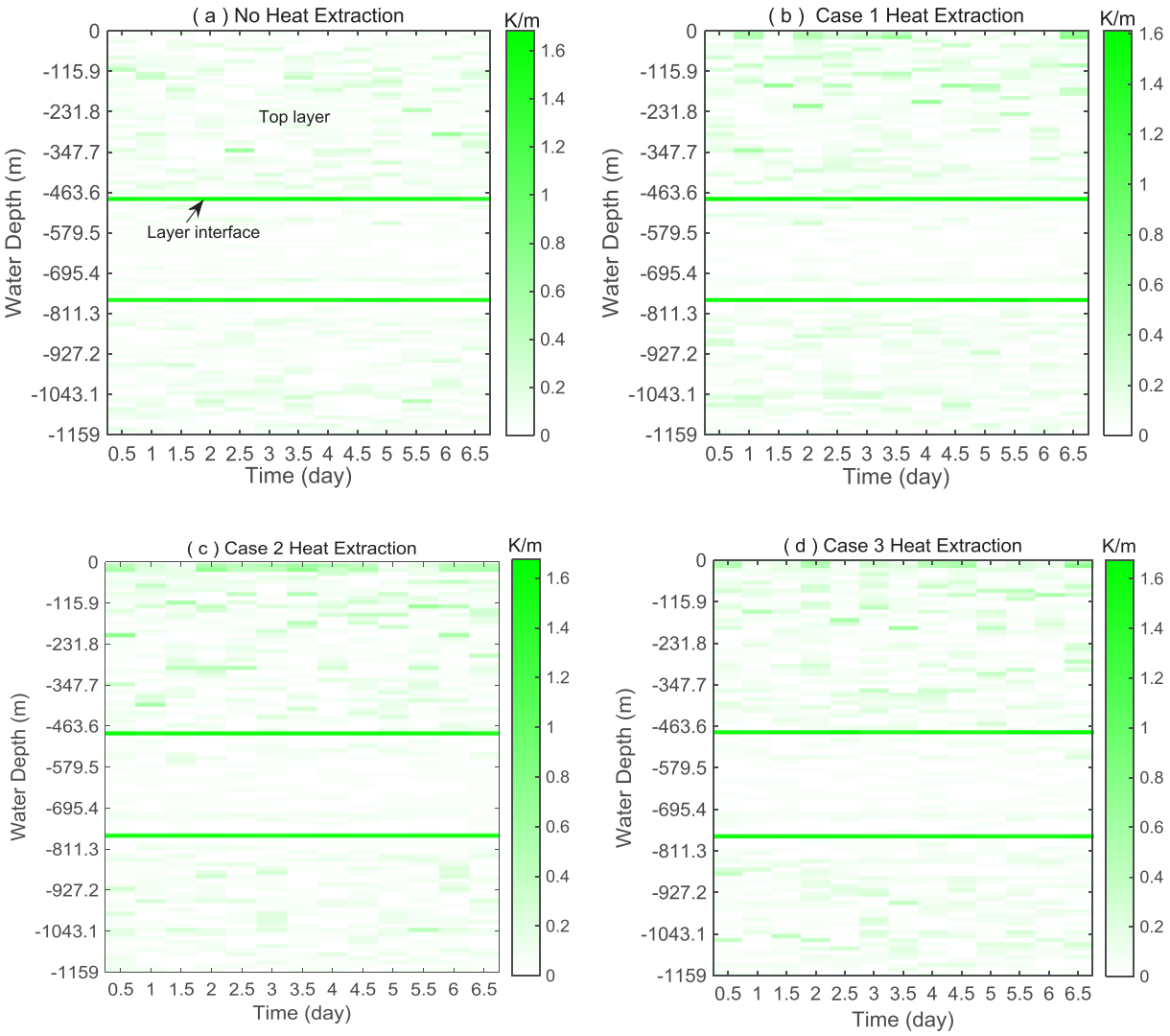

Fig. 15. Evolution of the absolute vertical temperature gradient along the center axis of Hancock Shaft 2 with and without heat extraction: (a) no heat extraction, (b) Case 1, (c) Case 2, and (d) Case 3.

It is clear that a pumping rate over a hundred times of a commonly used one in Table 1 can significantly affect the stability of layers by breaking the layer interface (see Fig. 16c). Usually, such a high pumping rate is unnecessary for heating a building like the one in [18] with a building area of 1394 m^2 because a relatively pumping rate of 0.0014 m^3/s is enough. However, such a high pumping rate can indirectly help evaluate heating a single building in the long term and can be possible in a more aggressive heating application with more buildings. 0.284 m^3/s is two-hundred times of 0.0014 m^3/s used in [18], which means that energy is recovered for heating two-hundred buildings for a week (i.e., large-scale). If a single building needs heating for five-month (20 weeks) in a year, heating this building with mine water by 10 years under continuous heat extraction will approximately result in a temperature reduction of 2 K (see temperatures marked in blue in Fig. 17a) compared to the original temperature of 283.3 K, which further validates the reliability of this energy innovation. However, for such large-scale energy applications, the design of the energy recovery system needs to be carried out based on a clear understanding of the interaction between the pumping rate and the behavior of the natural energy reservoir using methods such as the one presented in this study.

The above estimation might not be that accurate for real energy applications in long-term heat extraction. Therefore, further research is still needed to evaluate the long-term performance of heat extraction in several years, especially its influence on the stability of thermohaline stratification that dominates the natural heat and mass transport in real mine water bodies.

5. Conclusions

This study simulates transient heat extraction from a single mine shaft for heating using a unique numerical framework, in which the natural heat and mass transport in mine water dominated by thermohaline stratification was considered for the first time. The simulation results showed that, when the commonly-used pumping rates (i.e., 0.0014–0.03 m^3/s) are adopted, the pumping water for extracting heat via an open-loop heat pump system can alter the water temperature and the background water movement. However, the changes are only significant in the small local region close to the pumping location. Heat extraction has a negligible effect on the overall water temperature distributions and overall background water movement. The simulated outlet water temperatures almost remain unchanged, leading to a very stable water temperature available to heat pumps for extracting heat. These results are consistent with those measured in real applications and thus confirm the high efficiency and reliability of the energy application for heating using the simulations.

Discussions on simulation results also revealed that the stability of

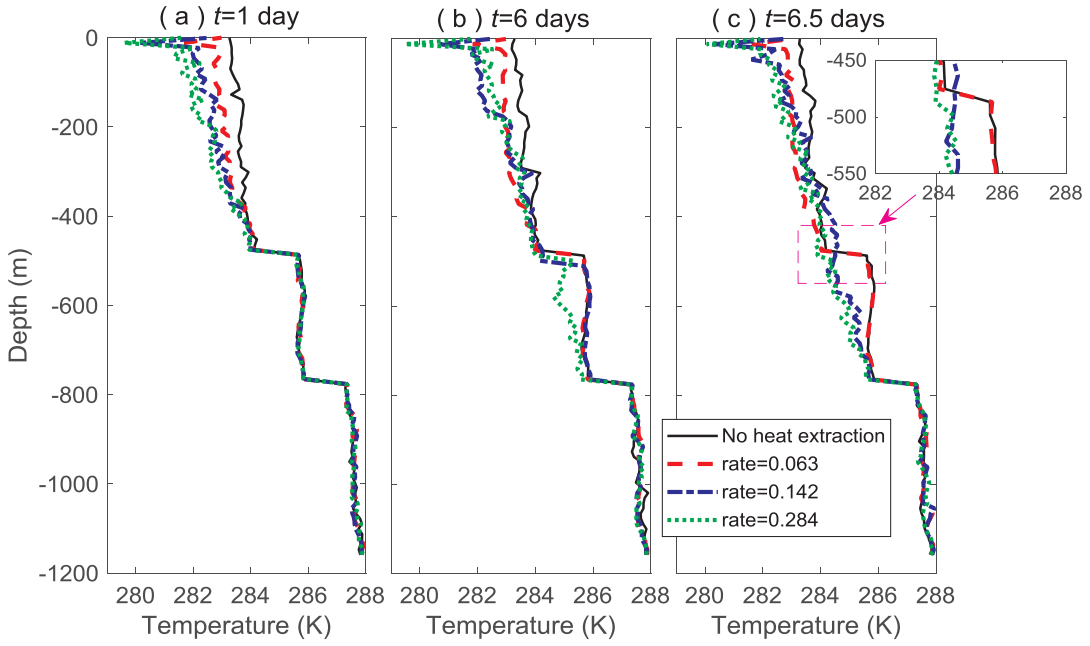

Fig. 16. Temperature distributions along the center axis of Hancock Shaft 2 with and without heat extraction at (a) 1 day, (b) 6 days, and (c) 6.5 days.

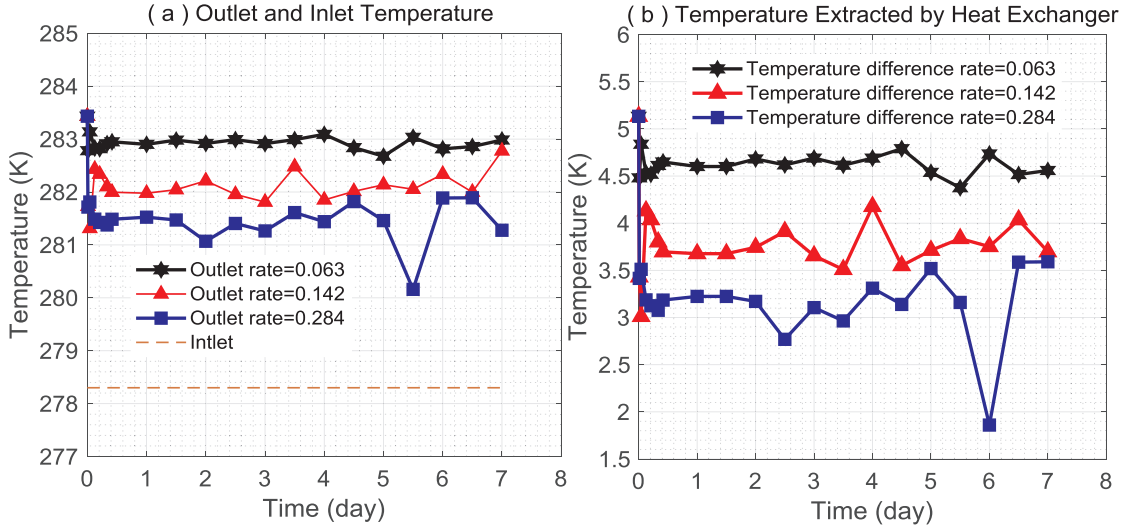

Fig. 17. Mine water temperatures at the inlet and outlet (a) temperature variations and (b) temperature reductions through the heat exchanger.

thermohaline stratification is negligibly influenced by continuous heat extraction because of the small pumping velocity and the long distance between the pumping location and the interface of neighboring layers. However, in further simulations where the pumping rate becomes a hundred times of a normal one, heat extraction can break the layer interface. The original stratified temperature distribution will turn to a linear distribution in a certain depth range in the simulations. This will cause major changes to the water temperature available to heat pumps and consequently the practice for the whole geothermal energy system.

This study successfully reproduces the key process in geothermal energy recovery with mine water and reveals the relationship between a key energy recovery parameter, i.e., pumping rate, and the behavior of the natural energy reservoir dominated by thermohaline stratification. Analyses with different values for the pumping rate confirm the sustainability of existing small-scale projects (low pumping rate) and identify a key issue for future large-scale applications (high pumping rate). This study also provides a tool for analyzing and predicting the efficiency and sustainability of the energy application.

Declaration of Competing Interest

There is no conflict of interest.

Acknowledgments

We acknowledge the support from Open Research Fund Program of Key Laboratory of Metallogenic Prediction of Nonferrous Metals and Geological Environment Monitoring (Central South University), Ministry of Education (Grant No. 2019YSJS01).

References

[1] Kabalci E. Design and analysis of a hybrid renewable energy plant with solar and wind power. Energy Convers Manage 2013;72:51–9.
[2] Cheng M, Zhu Y. The state of the art of wind energy conversion systems and technologies: a review. Energy Convers Manage 2014;88:332–47.
[3] Dias MO, Ensinas AV, Nebra SA, Maciel Filho R, Rossell CE, Maciel MRW. Production of bioethanol and other bio-based materials from sugarcane bagasse: integration to conventional bioethanol production process. Chem Eng Res Des

2009;87:1206–16.
[4] Sipahutar R, Bernas SM, Imanuddin MS. Renewable energy and hydropower utilization tendency worldwide. Renewable Sustainable Energy Rev 2013;17:213–5.
[5] Fridleifsson IB. Geothermal energy for the benefit of the people. Renewable Sustainable Energy Rev 2001;5:299–312.
[6] Franco A, Vaccaro M. A combined energetic and economic approach for the sustainable design of geothermal plants. Energy Convers Manage 2014;87:735–45.
[7] Barbier E. Geothermal energy technology and current status: an overview. Renewable Sustainable Energy Rev 2002;6:3–65.
[8] Lund J, Sanner B, Rybach L, Curtis R, Hellström G. Geothermal (ground-source) heat pumps-a world overview. GHC Bull 2004;25:1–10.
[9] Hepbasli A, Kalinci Y. A review of heat pump water heating systems. Renewable Sustainable Energy Rev 2009;13:1211–29.
[10] Ramos EP, Breede K, Falcone G. Geothermal heat recovery from abandoned mines: a systematic review of projects implemented worldwide and a methodology for screening new projects. Environ Earth Sci 2015;73:6783–95.
[11] Verhoeven R, Willems E, Harcouët-Menou V, De Boever E, Hiddes L, Optveld P. Minewater 2.0 project in Heerlen the Netherlands: transformation of a geothermal mine water pilot project into a full scale hybrid sustainable energy infrastructure for heating and cooling. Energy Procedia 2014;46:58–67.
[12] Watzlaf GR, Ackman TE. Underground mine water for heating and cooling using geothermal heat pump systems. Mine Water Environ 2006;25:1–14.
[13] Jessop AM, MacDonald JK, Spence H. Clean energy from abandoned mines at Springhill, Nova Scotia. Energy Sources 1995;17:93–106.
[14] Rottluff F. Neue Warmepumpenanlage im Besucherbergwerk Zinngrube Ehrenfriedersdorf. Geotermische Energie 1998;21:811.
[15] Burke T. The use in Scotland of flooded mine workings as a source of geothermal energy. Geothermal Energy in Underground Mines. 2002. p. 191–200.
[16] Burnside N, Banks D, Boyce A. Sustainability of thermal energy production at the flooded mine workings of the former Caphouse Colliery, Yorkshire, United Kingdom. Int J Coal Geol 2016;164:85–91.
[17] Behrooz BS, Elianne D, Jan- VB. Jaap Geothermal use of deep flooded mines. International symposium on post-mining, Nancy, France. 2008. p. 1–10.
[18] Bao T, Meldrum J, Vitton CGS, Liu Z, Bird K. Geothermal energy recovery from deep flooded copper mines for heating. Energy Convers Manage 2019;183:604–16.
[19] Al-Habaibeh A, Athresh AP, Parker K. Performance analysis of using mine water from an abandoned coal mine for heating of buildings using an open loop based single shaft GSHP system. Appl Energy 2018;211:393–402.
[20] Athresh AP, Al-Habaibeh A, Parker K. The design and evaluation of an open loop ground source heat pump operating in an ochre-rich coal mine water environment. Int J Coal Geol 2016;164:69–76.
[21] Menéndez J, Ordóñez A, Álvarez R, Loredo J. Energy from closed mines: underground energy storage and geothermal applications. Renewable Sustainable Energy Rev 2019;108:498–512.
[22] Petričko P, Kupka D, Koloničný J, Richter A. Economy of heat recovery from mining water in Ostrava region conditions. MATEC Web of Conferences. 2018.
[23] Menéndez J, Ordónez A, Fernández-Oro JM, Loredo J, Díaz-Aguado MB. Feasibility analysis of using mine water from abandoned coal mines in Spain for heating and cooling of buildings. Renewable Energy 2019;146:1166–76.
[24] MaJolepszy Z. Modelling of geothermal resources within abandoned coal mines, upper silesia, Poland. Geothermal training programme, Reykjavik, Iceland. 1998. p. 217–38.
[25] Bailey M, Gandy C, Watson I, Wyatt L, Jarvis A. Heat recovery potential of mine water treatment systems in Great Britain. Int J Coal Geol 2016;164:77–84.
[26] Jardón S, Ordóñez A, Alvarez R, Cienfuegos P, Loredo J. Mine water for energy and water supply in the Central Coal Basin of Asturias (Spain). Mine Water Environ 2013;32:139–51.
[27] Navarro A, Carulla N. Evaluation of geothermal potential in the vicinity of the flooded Sierra Almagrera Mines (Almeria, SE Spain). Mine Water Environ 2018;37:137–50.
[28] Loredo C, Ordóñez A, Garcia-Ordiales E, Álvarez R, Roqueñi N, Cienfuegos P, et al. Hydrochemical characterization of a mine water geothermal energy resource in NW Spain. Sci Total Environ 2017;576:59–69.
[29] Andrés C, Ordóñez A, Álvarez R. Hydraulic and thermal modelling of an underground mining reservoir. Mine Water Environ 2017;36:24–33.
[30] Raymond J, Therrien R. Low-temperature geothermal potential of the flooded Gaspé Mines, Québec, Canada. Geothermics 2008;37:189–210.
[31] Raymond J, Therrien R. Optimizing the design of a geothermal district heating and cooling system located at a flooded mine in Canada. Hydrogeol J 2014;22:217–31.
[32] Madiseh GS, Ghomshei MM, Hassani F, Abbasy F. Sustainable heat extraction from abandoned mine tunnels: a numerical model. J Renewable Sustainable Energy 2012;4:1–16.
[33] Thornton R. Convection mechanisms for geothermal heat exchangers in a vertical mine shaft. Butte, MT, USA: Montana Tech of The University of Montana; 2012.
[34] Matas A, García-Carro F, Loredo J. Characterization of Laciana Valley District mine water as geothermal resource. E3S Web of Conferences. 2018. p. 01003.
[35] Wolkersdorfer C. Water management at abandoned flooded underground mines: fundamentals, tracer tests, modelling, water treatment. München, Germany: Springer Science & Business Media; 2008.
[36] Turner J. Double-diffusive phenomena. Annu Rev Fluid Mech 1974;6:37–54.
[37] Johnson K, Younger P. Hydrogeological and geochemical consequences of the abandonment of Frazer's Grove carbonate hosted Pb/Zn fluorspar mine, North Pennines, UK. Geological Society, London, Special Publications. 2002. p. 347–63.
[38] Reichart G, Vaute L, Collon-Drouaillet P, Buès MA. Modelling heat and salinity related convective processes in deep mining flooded wells. 11th International Mine Water Association Congress, Aachen, Germany. 2011. p. 183–7.
[39] Bao T, Liu Z, Meldrum J, Green C, Xue P, Vitton S. Field tests and multiphysics analysis of a flooded shaft for geothermal applications with mine water. Energy Convers Manage 2018;169:174–85.
[40] Bao T, Liu Z. Thermohaline stratification modeling with double-diffusive convection for geothermal energy recovery from flooded mines. Appl Energy 2019;237:566–80.
[41] Sezai I, Mohamad A. Double diffusive convection in a cubic enclosure with opposing temperature and concentration gradients. Phys Fluids 2000;12:2210–23.
[42] Radko T, Bulters A, Flanagan J. Campin J-M. Double-diffusive recipes. Part I: large-scale dynamics of thermohaline staircases. J Phys Oceanogr 2014;44:1269–84.
[43] Vallis GK. Atmospheric and oceanic fluid dynamics. Cambridge University Press; 2017.
[44] OpenFOAM. Openfoam programmer's guide. OpenFOAM Foundation: http://foamsourceforgenet/docs/Guides-a4/ProgrammersGuidepdf. 2011.
[45] Devolder B, Schmitt P, Rauwoens P, Elsaesser B, Troch P. A review of the implicit motion solver algorithm in OpenFOAM® to simulate a heaving buoy. 18th Numerical Towing Tank Symposium, Cortona, Italy. 2015.
[46] Lee JW, Hyun JM. Double diffusive convection in a cavity under a vertical solutal gradient and a horizontal temperature gradient. Int J Heat Mass Transfer 1991;34:2423–7.
[47] Abu-Nada E, Akash B, Al-Hinti I, Al-Sarkhi A, Nijmeh S, Ibrahim A, et al. Modeling of a geothermal standing column well. Int J Energy Res 2008;32:306–17.
[48] Al-Sarkhi A, Abu-Nada E, Nijmeh S, Akash B. Performance evaluation of standing column well for potential application of ground source heat pump in Jordan. Energy Convers Manage 2008;49:863–72.
[49] USGS. USGS mineral resources data system: https://mrdata.usgs.gov/mrds/map-commodity.html. 2018.
[50] Suárez F, Tyler SW, Childress AE. A fully coupled, transient double-diffusive convective model for salt-gradient solar ponds. Int J Heat Mass Transfer 2010;53:1718–30.
[51] Muffler P, Cataldi R. Methods for regional assessment of geothermal resources. Geothermics 1978;7:53–89.
[52] Kories H, Rüterkamp P, Sippel M. Field and numerical studies of water stratification in flooded shafts. Proceedings International Mine Water Association Symposium, Newcastle upon Tyne, UK. 2004. p. 149–59.